Nanopaleomagnetism of meteoritic Fe-Ni studied using X-ray photoemission electron microscopy - Supplementary material

1. Magnetically soft layer PEEM images

A magnetically soft layer (~80nm thick) formed across the sample surface during mechanical polishing (Bryson et al., 2014), and before it's removal, it's nanomagnetic state was imaged (Supplementary Fig. 1). The region studied and the orientation of the X-ray beam direction relative to that of the microstructural features were different to those studied in Fig. 3. Despite the signal in these images originating solely from the soft layer, features representative of the kamacite, tetrataenite rim, CZ and plessite are all identifiable. The kamacite and tetrataenite rim are multidomain, with larger domains in the kamacite, and these domains appear to bleed across their shared interface (Fig. 1a). The kamacite contains domains with positive, negative and close to zero intensity, suggesting the magnetisation in these regions is parallel, anti-parallel and perpendicular to the X-ray beam direction, respectively. The coarse CZ (Supplementary Fig. 1b) displays a particulate texture with less detail than that observed once the soft layer was removed. The signal retains its strength, although becomes more uniform, with increasing distance from the tetrataenite rim. Among the finest islands the CZ signal reverses sign (Fig. 1c). The plessite displays elongated lath-like magnetic domains. These magnetic structures correlate closely with the underlying microstructure of each region (Goldstein and Michael, 2006; Goldstein et al., 2009; Yang and Goldstein, 2005). This observation implies that the soft layer mimics, to some extent, the unaltered magnetic structure beneath it. Given the thickness of the soft layer, it is likely that this mirroring originates from stray fields which imprint the CZ domain pattern into the soft layer.

A map of the in- and out-of-plane components of magnetisation was acquired by measuring the PEEM signal at 5 different sample rotation angles. As the sample rotates, the projection of the magnetisation onto the X-ray direction varies sinusoidally. After aligning the 5 images, the in- and out-of-plane components of magnetisation were deduced by fitting a sin function with a variable offset to the measured value at each pixel. The position of the maximum of this fitted wave represents the in-plane angle of the magnetisation relative to the X-ray direction, and the offset value relates directly to the strength of the out-of-plane component. The results of this analysis (Supplementary Fig. 2) show that the tetrataenite rim is multidomain, displaying striped domain patterns. The coarse CZ signal appears particulate, suggesting that differing easy axes populate the tetrataenite islands. In the finer CZ, the dominant signal is perpendicular to the tetrataenite rim direction, corresponding to the orientation of easy axis 1. The out-of-plane component for the finer CZ (Fig. 2b) is weak (which is to be expected given the magnetically soft nature of the surface being studied) but clearly demonstrates a dominant positive signal. In the finest CZ there is a reversal of both the in- and out-of-plane component of the magnetisation, implying that the interface between the two regions is a magnetic domain wall.

The domain patterns in the tetrataenite rim, CZ and plessite respond to magnetic field of ˜100 mT (Fig. 3). This behaviour is attributed to the response of the magnetically soft layer to the applied field, rather than the intrinsic response of the CZ which is known to have a much higher coercivity (Bryson et al., 2014; Uehara et al., 2011). The magnetically soft layer has been observed using electron holography (Bryson et al., 2014) to have a low coercivity ($\ll$200 mT). On increasing the strength of the applied magnetic field (Supplementary Fig. 3a, b, c), a domain wall starts sweeping towards the tetrataenite rim. Note the fine-scale domain patterns observed as the domain wall sweeps towards the coarse CZ (Supplementary Fig. 3b), providing strong evidence of an interaction between the soft layer and the underlying magnetic state of the CZ. The soft layer can be thought of as a multidomain magnetic structure and so, with the application of an applied field, the magnetic domain walls moves easily. There is, however, a clear imprint of the underlying magnetic domain pattern in the soft layer, demonstrated by the recreation of identical remanence states after each application of various applied fields (Supplementary Fig. 3a, d).

2. Compositional Maps

5 µm compositional maps of the kamacite, tetrataenite rim and CZ were generated by utilising linearly polarised X-rays tuned to the Ni and Fe $L_{2,3}$ absorption edges. The Ni composition is plotted in Supplementary Fig. 4, both with and without the magnetically soft layer. Before the soft layer removal (Supplementary Fig. 4b) the composition across the CZ is relatively constant, but displays a steady and expected decrease in Ni content with increasing distance from the tetrataenite rim once this layer has been removed (Fig. 4a). This observation suggests that the composition of the material is altered slightly during soft layer formation. Compositional variations in the CZ are expected at a fine scale due to the differences in composition between the island and the matrix phase. Note that the compositional variations in the CZ (Supplementary Fig. 4a) occur on a finer length scale that the size of the magnetic domains (Fig. 3), consistent with the suggestion that each magnetic domain comprises a cluster of several tetrataenite islands with the same easy axis orientation.

3. Micromagnetics

Micromagnetic simulations were performed using the Landau-Lifshitz-Gilbert equation (Scheinfein, 1997) both with and without a magnetically soft surface layer on top of the sample. The micromagnetic properties for tetrataenite were: M_s = 1300 emu/cm^3; A = 1.9 µerg/cm; K = 13700000 erg/cm^3, and for ordered Fe_3Ni and the soft layer: M_s = 1390 emu/cm^3; A = 1.5 µerg/cm; K = 0 erg/cm^3. The simulations without the soft layer were used to provide representative magnetisation values to generate the model magnetic nanostructures. These values were calculated by averaging the simulation magnetisation values for each of the three easy axis orientations. The value of the matrix magnetisation in the micromagnetic simulations was dependent upon the magnetisation of the two islands encasing the matrix phase. The average matrix magnetisation values were taken from these simulations, and used in the model nanostructure with the dependence on the neighbouring island magnetisation. The simulations with the soft layer (Supplementary Fig. 5) were used to investigate the pattern adopted by the soft layer, and the extent to which this pattern reflected that of the underlying CZ magnetisation. The simulation results show that the out of plane component of the soft layer (Supplementary Fig. 5b) is significantly reduced compared to that of the

underlying CZ (Supplementary Fig. 5a), which is expected given the magnetically soft nature of the layer and the stray magnetic field generated by the surface. This observation is in agreement with the experimental results (Supplementary Fig. 2b). The in-plane component appears to be a low resolution reflection of the CZ magnetisation (Supplementary Figs. 5c & d). The shape and size of magnetic domains in the CZ and soft layer are similar, although the detail in the island and matrix nanostructure and the signal originating from smaller lone islands is lost in the soft layer. These results prove that it is valid to consider the soft layer has an approximate mirror of the underlying unaltered CZ, and the mechanism of communication between the soft layer and CZ is stray magnetic fields. As the stray field originating from the islands is expected to decrease as the island diameter decreases, the imprint into the soft layer is also expected to decrease with island size, explaining the more uniform signal observed with increasing distance from the tetrataenite rim.

4. Magnetic Force Microscopy

Magnetic Force Microscopy (MFM) maps the magnetic force gradient $\partial F_z/\partial z$ between the sample and the magnetic tip of a cantilever beam oscillating at resonance frequency f_0 along the normal direction z to the sample surface. During a cantilever oscillation, the magnetic tip probes the sample magnetic stray field gradient $\partial B_z/\partial z$ and therefore feels an inhomogeneous force which, acting as an additional stiffness, shifts the resonance frequency of the beam by an amount $\Delta f \ll f_0$. If, for simplicity, the tip is assumed to be a magnetic dipole of magnitude $m = m_z$ and both sample and tip are supposed to be rigid (i.e. reciprocal perturbations of their magnetic states are negligible) then the frequency shift is:

$$\frac{\Delta f}{f_0} \propto \frac{\partial F_z}{\partial z} \propto m_z \frac{\partial^2 B_z}{\partial z^2} \tag{1}$$

An MFM scan records either the frequency shift Δf (if the cantilever resonance frequency is tracked by a feedback loop) or the phase shift $\Delta\varphi \propto \Delta f$ (if the cantilever is driven at constant frequency with no feedback loop). All the measurements presented here were carried out detecting the phase shift signal using the Lift mode of a Digital Instruments Dimension 3100 microscope. MFM measurements were performed scanning the sample with the soft layer still present at lift heights of 25–100 nm using low-moment ASYMFMLM Asylum Research tips coated with 15 nm of CoCr on cantilevers with stiffness 2 Nm^{-1}. Magnetic features as small as ~ 50 nm could be resolved at remanence after applying magnetic fields orientated normal to the plane of the sample between ±1T to investigate the island switching behaviour across the CZ. Initially a +1 T field was applied ex situ, followed by fields between -0.6 to -1 T in 0.1 T increments. Positive fields were then applied, and produced consistent results with the negative fields. The features observed in the MFM signal (Supplementary Fig. 6) are all reminiscent of those observed with the PEEM imaging (Fig. 3). Note the increase in signal strength in the finest CZ. The CZ MFM signal displays a speckled texture, consistent with the island nanostructure (Supplementary Fig. 7a). After an applied field of -0.6 T (Supplementary Fig. 7b) the signal in the coarse CZ changes relative to that observed after a 1 T applied field (Supplementary Fig. 7a), and between -0.7 T and -1 T (Supplementary Figs. 7c, d, e & f) the intermediate CZ signal decreases in intensity, while the finest CZ appears to remain constant at all applied field values. As the applied field strength is increased, the region of low contrast shifts to smaller island diameters.

The pattern of magnetic switching can be explained self-consistently with the observations made from the PEEM results. The change in pattern in the coarse CZ is associated with a complete reversal of

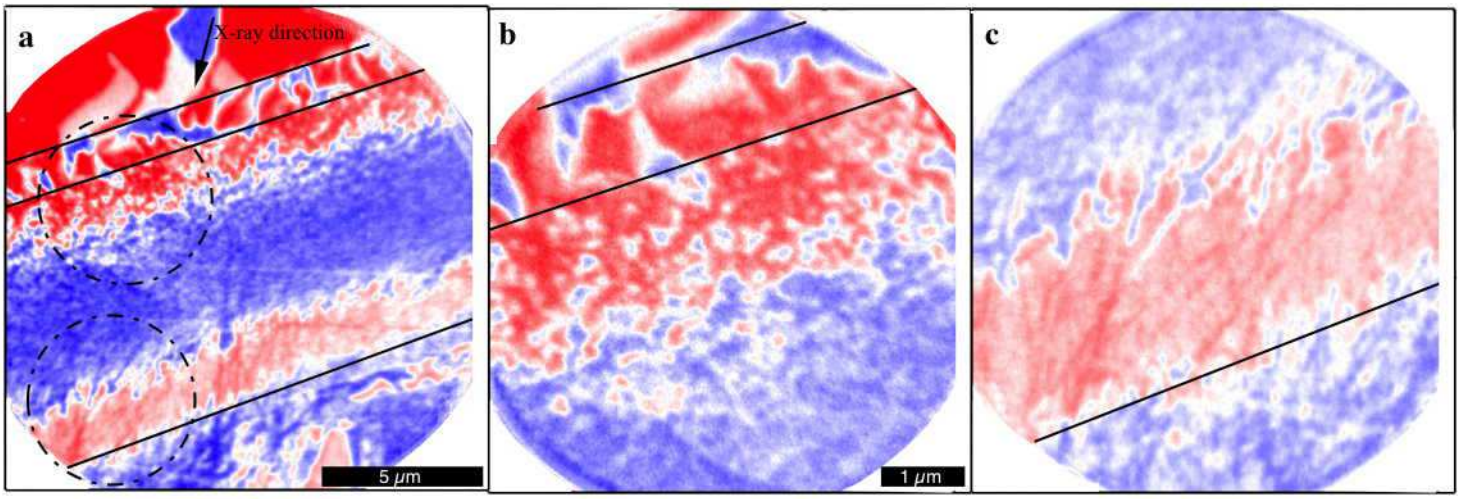

Supplementary Figure. 1: (a) 15 µm field of view image of the kamacite, tetrataenite rim, CZ and plessite with the magnetically soft layer still present on the sample surface. The boundaries between the phases have been included as solid black lines. The kamacite is at the top of the image, and the plessite at the bottom. The direction of the X-ray been has been included. (b,c) 5 µm field of view image of the tetrataenite rim and coarse CZ, and the fine CZ and plessite, respectively. The coarse and fine CZ regions correspond to the upper and lower dashed circles in (a), respectively.

the magnetisation with the applied field. Electron holography results (Bryson et al., 2014) show that the magnetisation in this region switches at an applied field value of around -0.5 T. As the range in switching field is relatively small in this region (Bryson et al., 2014), the stray fields emanating through the magnetically soft layer are expected to remain intense through switching, giving rise to the constant signal intensity observed experimentally in the coarse CZ. Electron holography results (Bryson et al., 2014) show that the intermediate to fine CZ magnetisation switches at applied field values $>$ -0.6T, and that this can occur over a relatively wide field range (from -0.6 T to $>$-1 T). The islands appear to switch in groups (as shown by the electron holography results and the roughness in the 1T contour observed in Fig. 3), thus the overall stray field emanating from the sample surface midway through switching may be relatively weak as the local fields generated by oppositely magnetised islands (partly) cancel. This weak stray field will result in the magnetism of the soft layer relaxing into the plane of the sample, generating the weak MFM signal. Once switching is complete, the islands will display a uniform out-of-plane magnetisation component, strengthening the stray fields and re-establishing the original MFM signal intensity. The weak intensity region shifts with increasing field strength due the coercivity increase with increasing distance from the tetrataenite rim. The finest region appears invariant as the applied field is not large enough to cause a change in the magnetisation direction. This region corresponds to the area below the 1 T contour in the PEEM images.

References

Bryson, J. F. J., Church, N. S., Kasama, T., Harrison, R. J., 2014. Nanomagnetic intergrowths in fe–ni meteoritic metal: The potential for time-resolved records of planetesimal dynamo fields. Earth and Planetary Science Letters 388, 237–248.

Goldstein, J. I., Michael, J., Jul 2006. The formation of plessite in meteoritic metal. Meteoritics and Planetary Science 41 (4), 553–570.

Goldstein, J. I., Scott, E. R. D., Chabot, N. L., Nov 2009. Iron meteorites crystallization, thermal history, parent bodies, and origin. Chemie der Erde - Geochemistry 69 (4), 293–325.

Horcas, I., Fernández, R., Gómez-Rodríguez, J. M., Colchero, J., Gómez-Herrero, J., Baro, A. M., 2007. Wsxm: A software for scanning probe microscopy and a tool for nanotechnology. Review of Scientific Instruments 78 (1), 013795–013807.

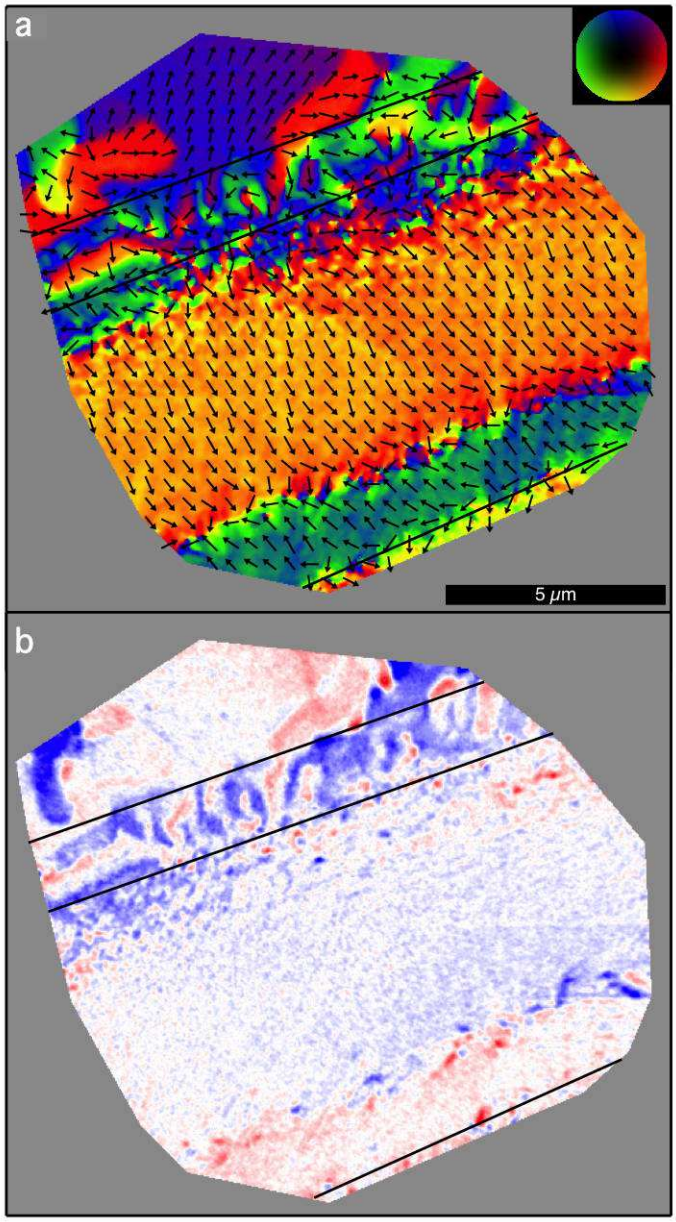

Supplementary Figure. 2: a) In-plane component of the magnetisation in Fig. 1(a). The in-plane component is represented as a colour (colour wheel inset) as well as arrows. b) Out-of-plane component of the magnetisation in Fig. 1(a). A clear change in both the in- and out-of-plane component of magnetisation is observed in the fine CZ. Blue: positive; red: negative.

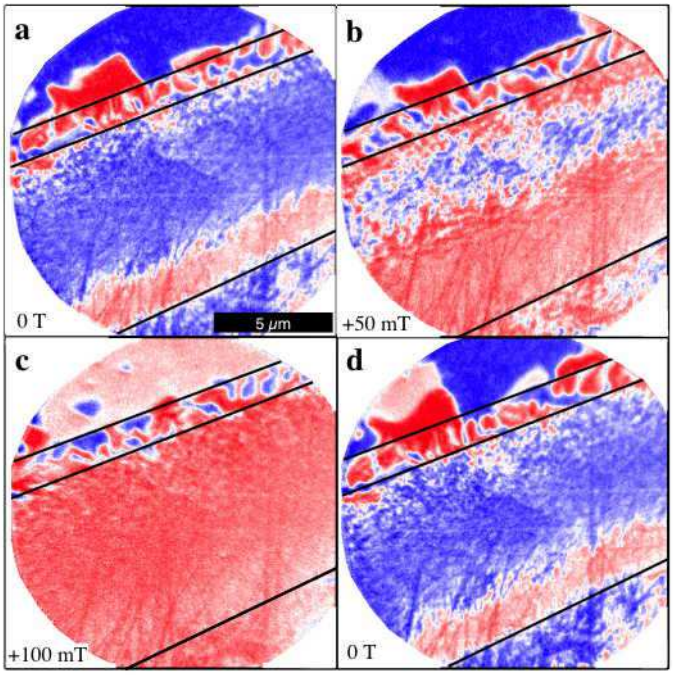

Supplementary Figure. 3: Remanence images obtained after the application of various in-plane fields in an area close to that in Fig. 1(a). (a) Magnetic domain pattern after zero applied field, demonstrating a qualitative similarity to Fig. 1(a). (b) Magnetic domain pattern after +50 mT. The domain wall representing the 1T contour has shifted towards the tetrtaenite rim, and the domain pattern of the kamacite, tetrataenite rim and plessite have all varied significantly. (c) Magnetic domain pattern after +100mT. The domain wall has swept completely through the CZ and the kamacite, tetrataenite rim and plessite all display further variations. (d) Magnetic domain pattern after -100 mT. Note a very similar domain pattern is established to that observed in (a). This similarity suggests the underlying magnetisation of the CZ influences the magneticallly soft layer, such that it (partially) mirrors the magnetic pattern of the CZ.

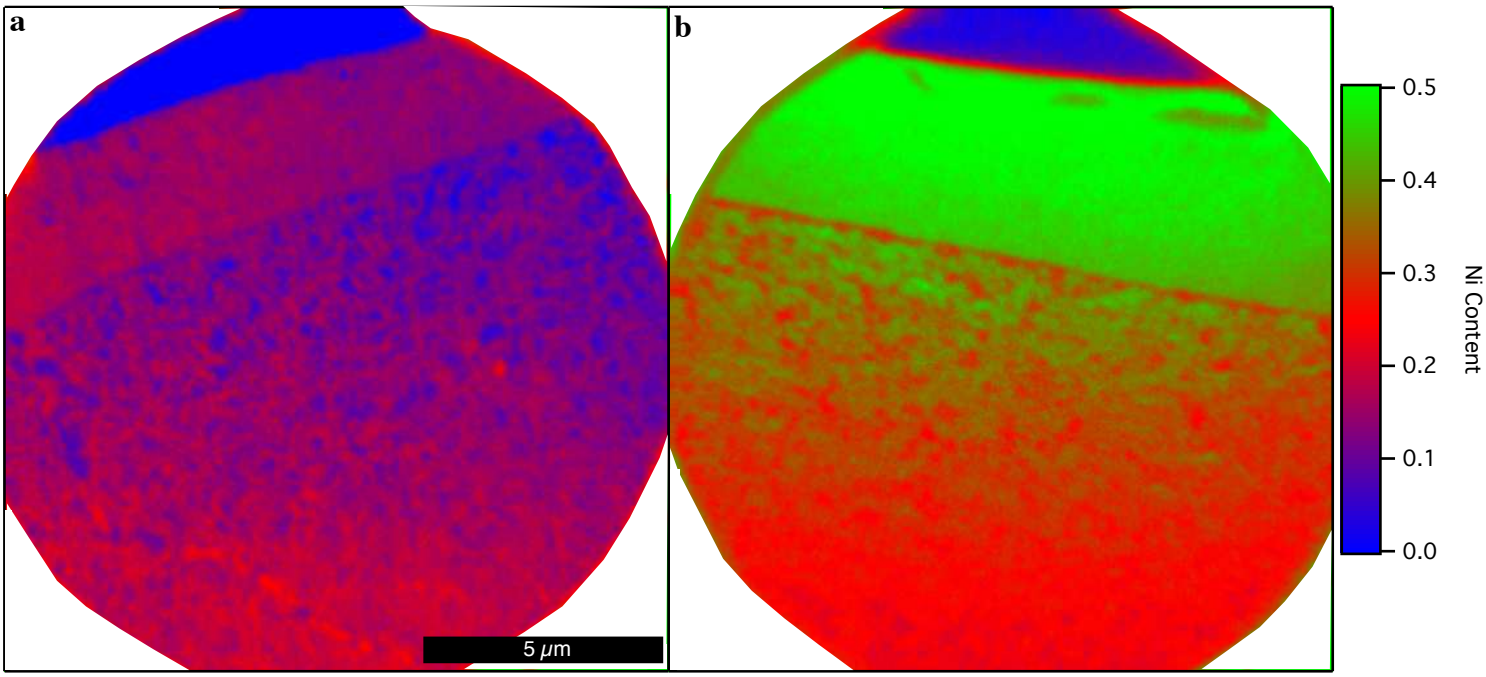

Supplementary Figure. 4: (a,b) Ni composition maps with and without the soft layer present respectively. The absolute values of the Ni composition are not calibrated to standard values, although the change in composition within each image still provides valid composition information. The change in composition across the CZ is flat with the soft layer and displays the expected decrease once this layer layer was removed. This observation suggests the composition of the CZ may be altered as the soft layer forms. The scale bar in (a) applies to both both images.

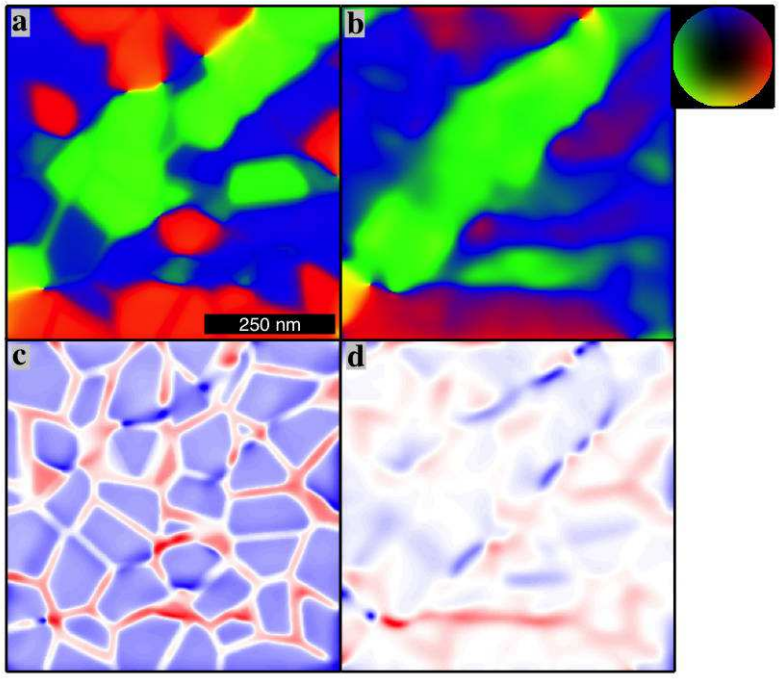

Supplementary Figure. 5: (a) In-plane component of the CZ from a micromagnetic simulation. (b) In-plane component of a soft layer atop the CZ in (a). A similar size, shape and intensity of domains is present in the two images, although (b) appears to be a lower resolution version of (a), with the details of the nanostructure and smaller lone islands lost. (c,d) Out-of-plane component of magnetisation corresponding to (a) and (b) respectively. The out-of-plane component of the soft layer is significantely reduced compared to that of the CZ itself, which is expected given the magnetically soft nature of the layer, and the stray fields generated at the surface.

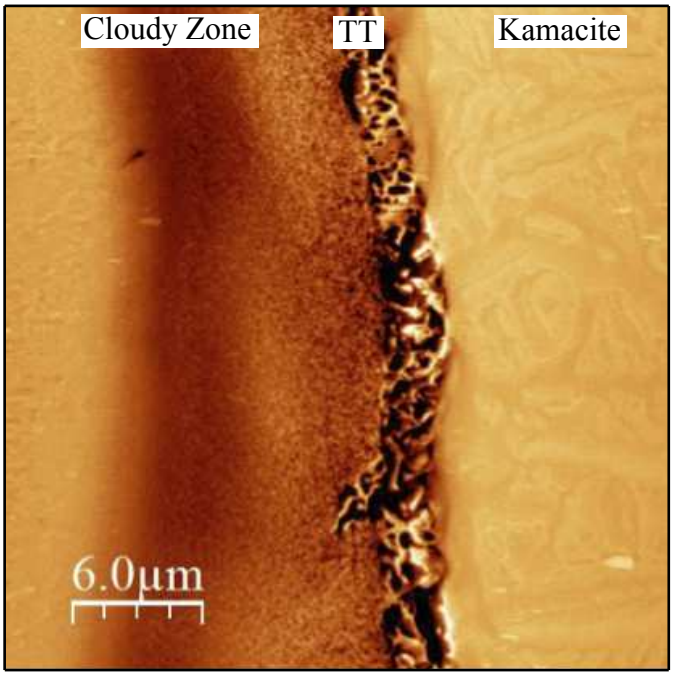

Supplementary Figure. 6: MFM image of the kamacite, tetrataenite rim (labelled as TT) and cloudy zone with the soft layer still atop the sample surface. The image was created using the software in Horcas et al. (2007). The CZ extends far to the left of the image where the signal intensity increases and it is possible that some of the plessite is also included in this region. Domains with weak contrast are visible in the kamacite. Smaller and more intense domains are visible in the tetrataenite rim. The CZ displays a speckled texture which decreases in intensity with increasing distance from the tetrataenite rim. In the fine CZ, the intensity increases. The plessite is visible on the far left of the image.

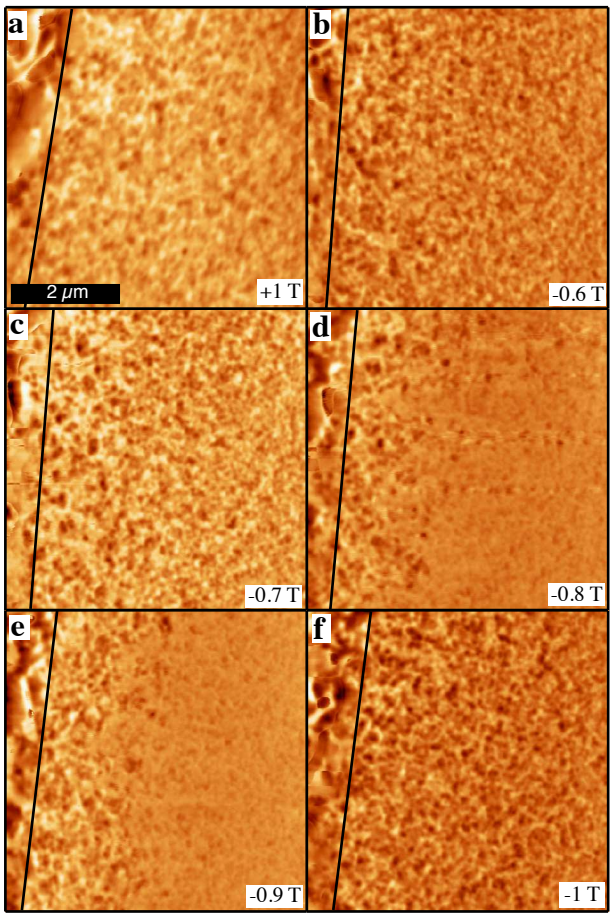

Supplementary Figure. 7: (a) MFM image at remanence after a +1 T field was applied normal to the plane of the sample. (b,c,d,e,f) Correspond to MFM signals at remanence after applied fields of -0.6 T, -0.7 T, -0.8 T, -0.9 T and -1 T respectively. All images have a 5.5 µm field of view and the island diameter decreases from left to right across the images. The position of the tetrataenite rim has been marked on with a solid black line. As the intermediate CZ switches, the MFM signal weakens due to the cancelation of the overall stray field as clusters of the islands reverse. Images were created using the software in by Horcas et al. (2007).

Scheinfein, M., 1997. Llg micromagnetic simulator. http://llgmicro.home.mindspring.com.
Uehara, M., Gattacceca, J., Leroux, H., Jacob, D., van der Beek, C. J., Jan 2011. Magnetic microstructures of metal grains in equilibrated ordinary chondrites and implications for paleomagnetism of meteorites. Earth and Planetary Science Letters 306 (3-4), 241–252.
Yang, J., Goldstein, J. I., Apr 2005. The formation of the widmanstatten structure in meteorites. Meteoritics and Planetary Science 40 (2), 239–253.